JACS
JOURNAL OF THE AMERICAN CHEMICAL SOCIETY
Communication
pubs.acs.org/JACS

Four-Component Supramolecular Nanorotors

Soumen K. Samanta and Michael Schmittel*

Center of Micro- and Nanochemistry and Engineering, Organische Chemie I, Universität Siegen, Adolf-Reichwein-Str. 2, D-57068 Siegen, Germany

Supporting Information

ABSTRACT: A family of supramolecular four-component nanorotors was quantitatively self-assembled from two different zinc(II) porphyrins: one representing the stator and the other the rotator with DABCO as an interconnecting axle and copper(I) ions. Rotational spinning in **ROT-1′** occurs at 97 000 s^{-1} at 25 °C but is virtually stopped at −75 °C. The activation vs binding data suggest that spinning is an intrasupramolecular process occurring to >99.9% without dissociation. Addition and removal of two further equiv of Cu^+ reversibly switches the mode of the stochastic rotation between pure 180° and mixed 90°/180° steps and reversibly regulates the speed between 97 000 and ∼80 000 s^{-1}.

In recent years, artificial molecular machinery[1] such as motors, tweezers, shuttles, and elevators[2] have received ample interest.[3] Despite the huge progress in recent years, there are many challenges left, for example to network two or more covalent machines and to interface their nanomechanical features. In contrast to man-made molecular machines, the nanomechanical ones from nature[4] such as F_0F_1-ATP synthase[4b] and bacterial flagella[4c] are formed by self-assembly. Thus nature's suggestion for nanomachines is unmistakable: its most sophisticated machineries with fascinating emergent properties only evolve from supramolecular heteroassemblies with covalent entities being weakly interlaced for superior nanomechanical operation and not from single covalent molecules.

In contrast to many reports covering fully covalent machines,[1−3,5] only few examples of artificial supramolecular devices are known,[6] such as the supramolecular valves by Stoddart and Zink,[6a,g] the nanomechanical tweezers by Aida,[6d] and Shionoya's[6b,f,h] four-component double-ball bearing complexes. While most examples constitute two- or three-component assemblies, we present here a family of new four-component supramolecular nanorotors that undergo fast stochastic rotary motion. Inspired by a successful self-assembly strategy developed in our laboratory,[7] the design is based on two dissimilar zinc porphyrins: one representing the rotator and the other one the stator[8] that are cofacially arranged about DABCO acting as a dynamic axle. However, to quantitatively heterosandwich DABCO between rotator **1** or **2** and stator **3** or **4** (Chart 1) by two axial N_{DABCO}−zinc porphyrin interactions (each contributing 27.6 kJ·mol^{-1}),[9] additional directing elements are required to preclude formation of homosandwich complexes. Thus, rotator (**1** or **2**) and stator (**3** or **4**) are furthermore anchored together at two trigonal $[Cu(phen)(py)]^+$ sites (*vide infra* for thermochemical data). Such heteroleptic pyridine and phenanthroline[10] (HETPYP) complexes arise in presence of copper(I) ions with the phenanthroline (phen) residues being provided from **3** or **4** and the pyridine/pyrimidine (py) units supplied by rotator **1** or **2**.

Chart 1. (A) Ligands 1−4 and (B) Cartoon Representation of Nanorotors

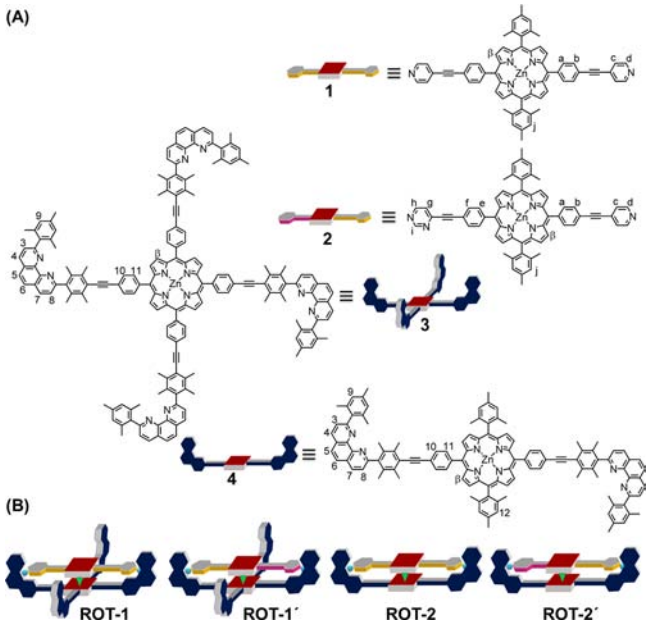

To prepare the four-component aggregate **ROT-1** = $[Cu_2(\mathbf{1})(\mathbf{3})(DABCO)]^{2+}$ (Figure 1A) by self-assembly,[7,11] ligand **3**[12] was first treated with 2 equiv of $[Cu(CH_3CN)_4]PF_6$ in dry DCM. In principle, the Cu^+ ions may occupy either 5,10- (*syn*), 5,15- (*anti*) or even three or four phenanthroline binding sites on platform **3**, which should result in a statistical mixture due to rapid exchange. Indeed, protons 9-H at the phenanthroline residues are diagnostically shifted downfield from 6.92 (in ligand **3**) to 7.03 ppm furnishing a single signal for $[Cu_2(\mathbf{3})]^{2+}$ (Figure 1B). However, upon further addition of 1 equiv of DABCO and 1 equiv of ligand **1**[10a] in dry $CHCl_3$ followed by 3 h of reflux quantitative formation of the desired complex **ROT-1** was noticed. The two Cu^+ ions are now exclusively arranged in *anti*-positions. **ROT-1** was characterized by ^1H NMR, ESI-MS, ^{13}C NMR, and elemental analysis (see SI). The ^1H NMR displays two diagnostic methylene singlets at −4.54 and −4.57 ppm corresponding to the DABCO sandwiched between two different

Received: October 31, 2013
Published: December 3, 2013

dx.doi.org/10.1021/ja411011a | J. Am. Chem. Soc. 2013, 135, 18794−18797

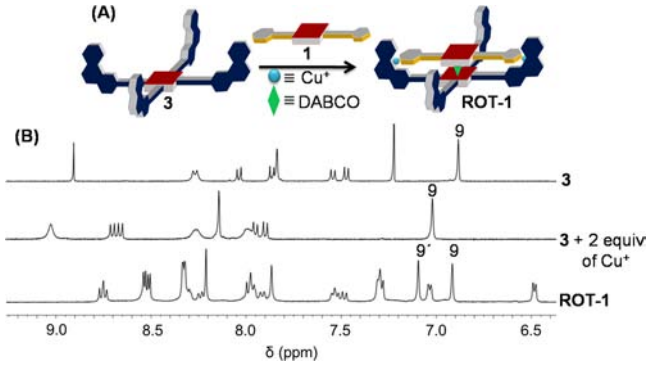

Figure 1. (A) Schematic synthesis of nanorotor **ROT-1**. (B) Partial ^{1}H NMR spectra of **3** ($CDCl_3$), **3** + 2 equiv of Cu^+ (CD_2Cl_2), and **ROT-1** (CD_2Cl_2: $CDCl_3$ = 9:1).

zinc porphyrins.[13] The pyridine protons c-H and d-H (Figure 1B) are shifted upfield to 7.04 and 6.47 ppm, which is characteristic for HETPYP complexation. In **ROT-1**, the highly symmetric tetrakisphenanthroline platform **3** loses its C_4 symmetry upon forming a complex with **1**, DABCO, and copper(I) ions. Diagnostically, **ROT-1** now exhibits in the ^{1}H NMR two different sets (1:1) of protons 9-H corresponding to rotator-loaded (at 7.10 ppm) and unloaded phenanthroline subunits (at 6.93 ppm), the latter resembling that in the copper-free ligand **3** (Figure 1B). An analogous behavior was observed for other phenanthroline protons in **ROT-1** as well, i.e., for 3-H, 4-H, 5-H, 6-H, 7-H and 8-H, when we compare **3** as isolated ligand with **3** in **ROT-1** (Table S1). The assembly is furthermore identified in the ESI-MS by a peak at 1845.8 Da corresponding to the doubly charged species **ROT-1** after loss of two counter-anions (PF_6^-). Finally, the ^{1}H DOSY proves **ROT-1** to be a single species in solution.

When 2 equiv of Cu^+ were added to **ROT-1** to generate **ROT-3** = $[Cu_2(\mathbf{ROT\text{-}1})]^{2+}$ (Figure 2), the set in the ^{1}H NMR

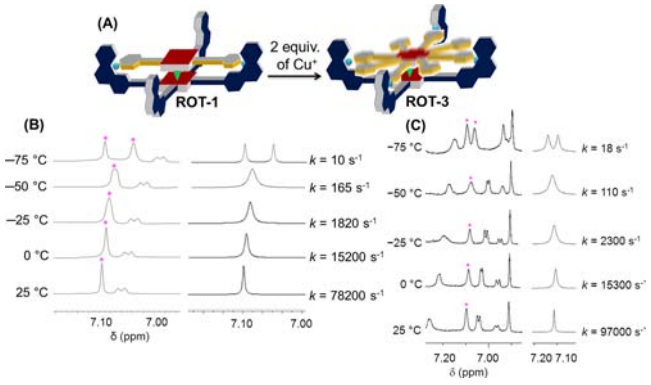

Figure 2. (A) Schematic synthesis of **ROT-3**. (B) Experimental (left) and simulated (right) ^{1}H NMR spectra of **ROT-3** ($CD_2Cl_2/CDCl_3$ = 9:1) at various temperatures. (C) Experimental (left) and simulated (right) ^{1}H NMR spectra of **ROT-1**′ ($CD_2Cl_2/CDCl_3$ = 9:1) at various temperatures.

representing the unloaded phenanthrolines of subunit **3** disappeared. All phenanthroline sites are now loaded with copper(I) ions and identical, as documented by a single signal for protons 9-H at 7.09 ppm. Moreover, protons c-H (7.07 ppm) and d-H (6.53 ppm) of the pyridine units are broadened and slightly shifted downfield (Figure S8). Two distinct singlets at −4.54 and −4.57 ppm represent the DABCO protons. An identical spectrum is received when ligand **3** was reacted with 4 equiv of Cu^+ followed by addition of 1 equiv of DABCO and 1 equiv of ligand **1** and refluxed for 3 h. Finally, ^{1}H DOSY proves $[Cu_2(\mathbf{ROT\text{-}1})](PF_6)_2$ to be a single species in solution.

The highly symmetric structure of **ROT-3** as derived from the ^{1}H NMR and the broadened resonances suggests that rotator **1** rapidly oscillates between the two pairs of orthogonal copper(I)-loaded phenanthroline stations of stator **3** at 25 °C. Insight into the dynamics of this spinning is obtained by cooling **ROT-3** to low temperature. While at 25 °C proton 9-H of **ROT-3** exhibits a single signal at 7.09 ppm, the spectrum displays two singlets of equal intensities at −75 °C (Figure 2).[14] The two signals at δ = 7.08 and 7.04 ppm are assigned to copper(I)-loaded phenanthroline stations that are coordinated and uncoordinated by the pyridine termini of **1**, respectively. As the temperature is raised to 25 °C, the two peaks gradually broaden and coalesce to a sharp singlet at 7.09 ppm.[15] This finding further supports our interpretation that at 25 °C all four copper(I)-loaded phenanthroline stations are chemically equivalent, due to fast spinning at 78 200 s^{-1}, while at −75 °C spinning is almost stopped. The activation parameters for the spinning process are determined to $\Delta H^{\ddagger}$ = 53.0 ± 0.2 kJ mol^{-1}, $\Delta S^{\ddagger}$ = 26.9 ± 0.7 J mol^{-1} K^{-1}, and $\Delta G^{\ddagger}_{25}$ = 45.0 kJ mol^{-1}.

For rotary oscillation in **ROT-3**, two pyridine−Cu^+ linkages[16] between rotator **1** and stator **3** need to dissociate requiring each ∼18.3 kJ mol^{-1} as binding of pyridine to a model complex $[Cu(phenAr_2)]^+$ in DCM was determined to log K = 3.2 ± 0.6, see Figure S31. The corresponding energy is thermally readily available at 25 °C suggesting that equally in **ROT-1** and the known **ROT-2**[10a] a rotary oscillation is populated. However, the high symmetry in both **ROT-1** and **ROT-2** prevents detection of such motion by ^{1}H NMR. As a consequence, we designed ligand **2**[12] as an unsymmetric rotator that has an $N_{pyridine}$−$N_{pyrimidine}$ separation of 2.9 nm, basically identical to that of the two pyridine termini in rotator **1**. Alike **ROT-1** and **ROT-2**, the four-component assembly **ROT-1**′ (or alternatively **ROT-2**′) was synthesized from a 1:1:2:1 mixture of **3** (or **4**),[13b] **2**,[12] Cu^+, and DABCO and characterized in the same manner as **ROT-1** (see SI).

As predicted, at 25 °C the unsymmetric rotator **2** does not desymmetrize the two opposing copper(I)-loaded phenanthroline stations in both **ROT-1**′ and **ROT-2**′, suggesting rapid exchange of pyridine and pyrimidine termini on the NMR time scale. As before, the dynamics was evaluated using ^{1}H VT-NMR. Upon cooling **ROT-1**′ = $[Cu_2(\mathbf{2})(\mathbf{3})(DABCO)]^{2+}$ to −75 °C, protons 9-H of both copper-loaded phenanthroline stations split into two signals at 7.09 and 7.07 ppm (1:1) due to slow exchange. Those stations are now connected to the pyridine and pyrimidine terminus of rotator **2**.[16] Upon raising the temperature, the two peaks coalesce along with a slight downfield shift resulting in a sharp signal at 7.10 ppm at 25 °C. The singlet at 6.92 ppm assigned to protons 9-H of the copper(I)-free phenanthrolines remains constant over the whole temperature range advocating against translocation of Cu^+ between the two orthogonal pairs of phenanthrolines and thus for pure 180° rotational oscillations. Alike the dynamics in **ROT-2**′ = $[Cu_2(\mathbf{2})(\mathbf{4})(DABCO)]^{2+}$ was investigated (Table 1). The comparable activation parameters and rotational frequencies of nanorotors **ROT-1**′ and **ROT-2**′ indicate that copper-free phenanthroline sites, as present in **ROT-1**′, do not influence the rotation. Therefore, the observed spinning in the unsymmetric nanorotors suggests a similar, nondetectable rotation in the symmetric nanorotors **ROT-1** and **ROT-2**.

dx.doi.org/10.1021/ja411011a | J. Am. Chem. Soc. 2013, 135, 18794−18797

Table 1. Experimental Rotational Frequency at 25 °C and the Activation Parameters of the Nanorotors

nanorotors[a]	$\Delta H^{\ddagger}$ (kJ mol^{-1})	$\Delta S^{\ddagger}$ (J mol^{-1} K^{-1})	$\Delta G^{\ddagger}_{25}$ (kJ mol^{-1})	k_{25} (s^{-1})
ROT-1′	47.5 ± 0.6	22.0 ± 0.8	41.0	97 000
ROT-2′	47.1 ± 0.5	23.0 ± 0.8	40.2	96 300
ROT-3	53.0 ± 0.2	26.9 ± 0.7	45.0	78 200
ROT-3′	52.8 ± 0.4	31.0 ± 0.9	43.8	81 300

[a]Activation parameters could not be determined for **ROT-1** and **ROT-2** due to their symmetry.

When 2 equiv of Cu^+ were added to nanorotor **ROT-1′**, the new aggregate **ROT-3′** = $[Cu_2(\textbf{ROT-1}')]^{2+}$ formed as observed from NMR, alike **ROT-3** (Figure 3). The dynamics in **ROT-3′**

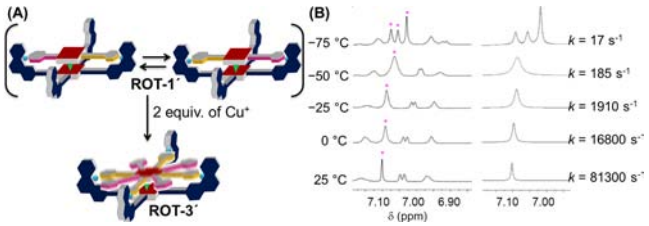

Figure 3. (A) Schematic synthesis of **ROT-3′** and a cartoon representation of the spinning in **ROT-1′** (180° steps) and **ROT-3′** (90°/180° steps). (B) Experimental (left) and simulated (right) ^{1}H NMR spectra of **ROT-3′** (CD_2Cl_2/$CDCl_3$ = 9:1) at various temperatures.

can be followed from ^{1}H VT-NMR that at −75 °C shows three sets (1:1:2) of phenanthroline mesityl protons (9-H) at 7.08, 7.06, and 7.03 ppm. Signals of equal intensities correspond to rotator-loaded phenanthroline stations while the singlet at 7.03 ppm is assigned to the rotator-free copper(I)-loaded stations. The slightly lower activation barrier $\Delta G^{\ddagger}_{25}$ = 43.8 kJ mol^{-1} and higher rotational frequency (k_{25} = 81300 s^{-1}) for the spinning motion in **ROT-3′** compared to **ROT-3** is expected because the Cu^+−pyrimidine detachment (15.9 kJ mol^{-1}; derived from log K = 2.78 ± 0.34 for binding of pyrimidine to $[Cu(phenAr_2)]^+$, see Figure S31) requires less energy than the Cu^+−pyridine dissociation (18.3 kJ mol^{-1}).

The observed exchange processes in all nanorotors may be rationalized by either intrasupramolecular spinning of rotators **1**,**2** against the stator or by a dissociation/reassociation mechanism (Figure 4). While intrasupramolecular rotation requires only detachment of the two pyridine and/or pyrimidine

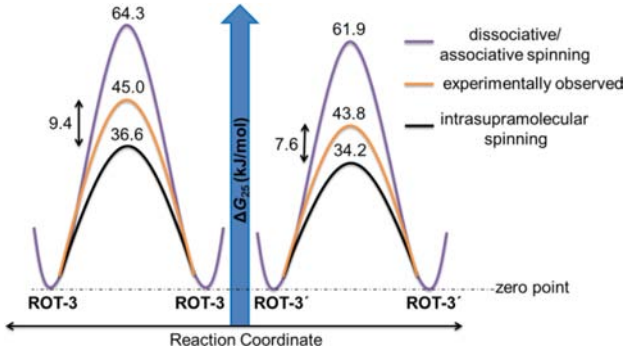

Figure 4. Schematic energy profiles of the rotational spinning in **ROT-3** and **ROT-3′** considering different mechanistic scenarios.

nitrogens of the rotator from the copper(I)-loaded phenanthroline stations,[16] the dissociation/association pathway additionally demands cleavage of at least one N_{DABCO}−zinc porphyrin interaction. The latter was determined as follows: analysis of the binding isotherm for **3**·DABCO by UV−vis using a 1:1 binding model furnishes the stoichiometric binding constant $K_{11} = 3.47 \times 10^5$ M^{-1} (log K = 5.54 ± 0.65, see Figure S32), which gives the microscopic binding constant $K_m = K_{11}/2 = 1.74 \times 10^5$ M^{-1}.[17] Thus, the binding constant $K_{11\leftrightarrow 12} = \alpha_{DABCO}K_m/2$ for the formation of the ternary complex $(\textbf{3})_2$·DABCO from the binary complex **3**·DABCO + **3** may be estimated as 0.70×10^5 M^{-1} using the cooperativity factor α_{DABCO} = 0.8 ± 0.2, as reported earlier. A binding constant of 0.70×10^5 M^{-1} for disruption of one DABCO−zinc porphyrin bond amounts to 27.7 kJ mol^{-1} in free energy at room temperature.[18] Accordingly, intrasupramolecular spinning requires a minimum energy barrier of 36.6 and 34.2 kJ mol^{-1} for nanorotors with symmetric rotator **1** and unsymmetric rotator **2**, respectively, while the dissociation/association mechanism would demand a minimum energy barrier of 64.3 and 61.9 kJ·mol^{-1} (Figure 4). Clearly, the experimental barriers $\Delta G^{\ddagger}_{25}$ as well as the low positive activation entropies (Table 1) point toward intrasupramolecular spinning (>99.9%) for all nanorotors. The small deviation of the experimental barrier from the ideal intrasupramolecular one based solely on thermodynamics (for example $\Delta\Delta G^{\ddagger}$ = 6.8 kJ mol^{-1} for **ROT-1′**) may arise from some cooperative effects of pyridine/pyrimidine−Cu^+ binding due to the perfect preorientation in the nanorotor.

Comparing the activation barriers for the spinning in the nanorotors shows that **ROT-3′** has a lower rotational frequency and thus higher barrier than **ROT-1′** by 2.8 kJ mol^{-1}, most likely due to statistical effects arising from nondirectional 90° vs 180° oscillatory leaps. The overall rotational process is furthermore complicated because the phenanthroline stations themselves constitute almost barrierless side rotors with the side rotators not necessarily oriented all-*syn* toward the main rotator **1** or **2** (see Figure S33). In the fully copper(I)-loaded systems **ROT-3** and **ROT-3′**, the metal ion in the rotator-free phenanthroline stations becomes coordinatively unsaturated once the rotator (**1** or **2**) has moved to the next pair of stations in the spinning. Thus, the set of rotator-free phenanthroline stations may rotate about the alkynyl groups of the stator. As a result, we expect **ROT-3** and **ROT-3′** to undergo mixed 90° vs 180° rotational moves, while **ROT-1** and **ROT-1′** operate by pure 180° oscillations. Importantly, removing Cu^+ from **ROT-3** and **ROT-3′** by adding 2 equiv of cyclam affords nanorotors **ROT-1** and **ROT-1′** operating along a pure 180° rotational mode (see SI).

In conclusion, we have synthesized a family of four-component supramolecular nanorotors that rotate in a stochastic oscillating manner about a dynamic hinge, resembling closely that in a rotary sprinkler. The spinning motion takes place by an intrasupramolecular pathway (>99.9%) as clearly demonstrated by kinetic and thermodynamic data. Moreover, addition and removal of metal ions allows reversible regulation of the speed (97 000 ↔ ~80 000 s^{-1}) of the nanorotors and their mode of rotation (pure 180° vs mixed 90°/180° leaps).

This self-assembly protocol constitutes a big step toward constructing fully operational machines—alike nature—through simply mixing dissimilar molecular components, an extremely versatile strategy that will propel the emerging fields of machine assemblies. Further speed regulation in nanorotors is currently underway.

dx.doi.org/10.1021/ja411011a | J. Am. Chem. Soc. 2013, 135, 18794−18797

■ ASSOCIATED CONTENT

Supporting Information

Experimental procedures and spectroscopic data. This material is available free of charge via the Internet at http://pubs.acs.org

■ AUTHOR INFORMATION

Corresponding Author

schmittel@chemie.uni-siegen.de

Notes

The authors declare no competing financial interest.

■ ACKNOWLEDGMENTS

We acknowledge generous funding by the DFG and the University of Siegen. We are very much indebted to Dr. T. Paululat (University of Siegen) for recording the low temperature NMR.

■ REFERENCES

(1) (a) *Molecular Catenanes, Rotaxanes and Knots*; Sauvage, J.-P., Dietrich-Buchecker, C., Eds.; Wiley-VCH: Weinheim, 1999. (b) Balzani, V.; Credi, A.; Raymo, F. M.; Stoddart, J. F. *Angew. Chem., Int. Ed.* **2000**, *39*, 3348. (c) Kay, E. R.; Leigh, D. A.; Zerbetto, F. *Angew. Chem., Int. Ed.* **2007**, *46*, 72.

(2) (a) Badjić, J. D.; Balzani, V.; Credi, A.; Silvi, S.; Stoddart, J. F. *Science* **2004**, *303*, 1845. (b) Muraoka, T.; Kinbara, K.; Aida, T. *Nature* **2006**, *440*, 512. (c) Ruangsupapichat, N.; Pollard, M. M.; Harutyunyan, S. R.; Feringa, B. L. *Nat. Chem.* **2011**, *3*, 53. (d) von Delius, M.; Geertsema, E. M.; Leigh, D. A.; Tang, D.-T. D. *J. Am. Chem. Soc.* **2010**, *132*, 16134. (e) Leblond, J.; Gao, H.; Petitjean, A.; Leroux, J.-C. *J. Am. Chem. Soc.* **2010**, *132*, 8544.

(3) (a) Jeon, W. S.; Kim, E.; Ko, Y. H.; Hwang, I.; Lee, J. W.; Kim, S.-Y.; Kim, H.-J.; Kim, K. *Angew. Chem., Int. Ed.* **2005**, *44*, 87. (b) Lang, T.; Guenet, A.; Graf, E.; Kyritsakas, N.; Hosseini, M. W. *Chem. Commun.* **2010**, *46*, 3508. (c) Haberhauer, G. *Angew. Chem., Int. Ed.* **2010**, *49*, 9286. (d) Kudernac, T.; Ruangsupapichat, N.; Parschau, M.; Maciá, B.; Katsonis, N.; Harutyunyan, S. R.; Ernst, K.-H.; Feringa, B. L. *Nature* **2011**, *479*, 208. (e) Schmittel, M.; De, S.; Pramanik, S. *Angew. Chem., Int. Ed.* **2012**, *51*, 3832.

(4) (a) Schliwa, M.; Woehlke, G. *Nature* **2003**, *422*, 759. (b) Yoshida, M.; Muneyuki, E.; Hisabori, T. *Nat. Rev. Mol. Cell Biol.* **2001**, *2*, 669. (c) Dreyfus, R.; Baudry, J.; Roper, M. L.; Fermigier, M.; Stone, H. A.; Bibette, J. *Nature* **2005**, *437*, 862.

(5) Ogi, S.; Ikeda, T.; Wakabayashi, R.; Shinkai, S.; Takeuchi, M. *Chem.—Eur. J.* **2010**, *16*, 8285.

(6) (a) Hernandez, R.; Tseng, H.-R.; Wong, J. W.; Stoddart, J. F.; Zink, J. I. *J. Am. Chem. Soc.* **2004**, *126*, 3370. (b) Hiraoka, S.; Shiro, M.; Shionoya, M. *J. Am. Chem. Soc.* **2004**, *126*, 1214. (c) Silvi, S.; Arduini, A.; Pochini, A.; Secchi, A.; Tomasulo, M.; Raymo, F. M.; Baroncini, M.; Credi, A. *J. Am. Chem. Soc.* **2007**, *129*, 13378. (d) Kai, H.; Nara, S.; Kinbara, K.; Aida, T. *J. Am. Chem. Soc.* **2008**, *130*, 6725. (e) Bhosale, S. V.; Chong, C.; Forsyth, C.; Langford, S. J.; Woodward, C. P. *Tetrahedron* **2008**, *64*, 8394. (f) Hiraoka, S.; Okuno, E.; Tanaka, T.; Shiro, M.; Shionoya, M. *J. Am. Chem. Soc.* **2008**, *130*, 9089. (g) Ferris, D. P.; Zhao, Y.-L.; Khashab, N. M.; Khatib, H. A.; Stoddart, J. F.; Zink, J. I. *J. Am. Chem. Soc.* **2009**, *131*, 1686. (h) Hiraoka, S.; Hisanaga, Y.; Shiro, M.; Shionoya, M. *Angew. Chem., Int. Ed.* **2010**, *49*, 1669.

(7) (a) Kishore, R. S. K.; Paululat, T.; Schmittel, M. *Chem.—Eur. J.* **2006**, *12*, 8136. (b) Mahata, K.; Saha, M. L.; Schmittel, M. *J. Am. Chem. Soc.* **2010**, *132*, 15933.

(8) Kottas, G. S.; Clarke, L. I.; Horinek, D.; Michl, J. *Chem. Rev.* **2005**, *105*, 1281.

(9) Ballester, P.; Oliva, A. I.; Costa, A.; Deyà, P. M.; Frontera, A.; Gomila, R. M.; Hunter, C. A. *J. Am. Chem. Soc.* **2006**, *128*, 5560.

(10) (a) Samanta, S. K.; Samanta, D.; Bats, J. W.; Schmittel, M. *J. Org. Chem.* **2011**, *76*, 7466. (b) Neogi, S.; Schnakenburg, G.; Lorenz, Y.; Engeser, M.; Schmittel, M. *Inorg. Chem.* **2012**, *51*, 10832.

(11) (a) Northrop, B. H.; Zheng, Y.-R.; Chi, K.-W.; Stang, P. J. *Acc. Chem. Res.* **2009**, *42*, 1554. (b) De, S.; Mahata, K.; Schmittel, M. *Chem. Soc. Rev.* **2010**, *39*, 1555. (c) Sun, Q.-F.; Iwasa, J.; Ogawa, D.; Ishido, Y.; Sato, S.; Ozeki, T.; Sei, Y.; Yamaguchi, K.; Fujita, M. *Science* **2010**, *328*, 1144. (d) Chakrabarty, R.; Mukherjee, P. S.; Stang, P. J. *Chem. Rev.* **2011**, *111*, 6810.

(12) Synthesis of ligands **2** and **3** will be published in due course.

(13) (a) Baldini, L.; Ballester, P.; Casnati, A.; Gomila, R. M.; Hunter, C. A.; Sansone, F.; Ungaro, R. *J. Am. Chem. Soc.* **2003**, *125*, 14181. (b) Schmittel, M.; Samanta, S. K. *J. Org. Chem.* **2010**, *75*, 5911.

(14) Splitting of 9-H at −75 °C due to *in* vs *out* mesityl protons after freezing mesityl rotation can be ruled out, because no splitting was observed for 9-H at the coordinated stations in **ROT-1** and **ROT-2** at −75 °C (see SI).

(15) Kajiwara, T.; Yokozawa, S.; Ito, T.; Iki, N.; Morohashi, N.; Miyano, S. *Angew. Chem., Int. Ed.* **2002**, *41*, 2076.

(16) As the binding energy of Cu^+ to phenanthroline is roughly double of that to pyridine, the rotary motion exclusively involves dissociation of pyridine from Cu^+.

(17) In the ensuing reaction scheme depicting all species involved in the equilibration of DABCO and zinc(II) porphyrin, the following data are of interest: the overall binding constant K_{12}, the individual constants K_{11} and $K_{11\leftrightarrow12}$, the microscopic binding constant K_m and the ligand cooperativity factor α_{DABCO}.

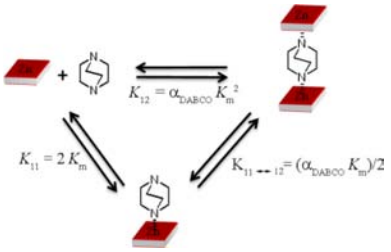

(18) As an approximation, we have used a dissociation energy 27.7 kJ mol^{-1} for the cleavage of all ternary complexes (**3** or **4**)·DABCO·(**1** or **2**) into the binary complexes, i.e., either (**3** or **4**)·DABCO + (**1** or **2**) or (**3** or **4**) + DABCO·(**1** or **2**), although both zinc porphyrin units are different in **ROT-1**, **ROT-2**, **ROT-1′**, and **ROT-2′**.